Foroutan et al., *BioImpacts.* 2025;15:30954
doi: 10.34172/bi.30954
https://bi.tbzmed.ac.ir/

Biosynthesis of sulfur quantum dots and cerium oxide nanoparticles for bioimaging and reactive oxygen species modulation in Y79 retinoblastoma cancer cells

Zahra Foroutan[1#], Sadaf Afshari[2#], Sajjad Njafi[3,4], Amir R. Afshari[5,6,7], Seyed Sajad Ahmadi[8], Seyedsina Nemati[2], Seyedeh Mozhdeh Mirzaei[1], Afsane Bahrami[9,10*]

[1]Department of Medical Biotechnology & Nanotechnology, Faculty of Medicine, Mashhad University of Medical Sciences, Mashhad, Iran
[2]Student Research Committee, Faculty of Dentistry, Mashhad University of Medical Sciences, Mashhad, Iran
[3]Neurosurgery Department, Neurovascular Section, Ghaem Hospital, Mashhad University of Medical Sciences, Mashhad, Iran
[4]Neurosurgical Department, Mazandaran University of Medical Sciences, Sari, Iran
[5]Department of Basic Sciences, Faculty of Medicine, Mashhad Medical Sciences, Islamic Azad University, Mashhad, Iran
[6]Natural Products and Medicinal Plants Research Center, North Khorasan University of Medical Sciences, Bojnurd, Iran
[7]Department of Physiology and Pharmacology, Faculty of Medicine, North Khorasan University of Medical Sciences, Bojnurd, Iran
[8]Department of Ophthalmology, Khatam-Ol-Anbia Hospital, Mashhad University of Medical Sciences, Mashhad, Iran
[9]Clinical Research Development Unit of Akbar Hospital, Faculty of Medicine, Mashhad University of Medical Sciences, Mashhad, Iran
[10]Clinical Research Development Unit, Imam Reza Hospital, Faculty of Medicine, Mashhad University of Medical Sciences, Mashhad, Iran

Article Info

Article Type:
Original Article

Article History:
Received: 8 Jan. 2025
Revised: 4 Mar. 2025
Accepted: 12 Mar. 2025
ePublished: 25 May 2025

Keywords:
Cerium oxide nanoparticles
Sulfur quantum dots
Retinoblastoma (Y79)
Green synthesis

Abstract

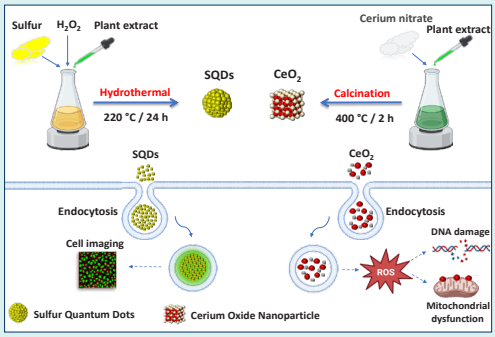

Introduction: Retinoblastoma is considered a common cancer in early childhood with a poor prognosis, and innovative strategies for early diagnosis and treatment are essential. The use of nanoparticles is one of the most efficient approaches among these strategies.

Methods: Sulfur quantum dots (SQDs) and cerium oxide nanoparticles (CeO_2) were synthesized through simple and eco-friendly green synthesis method using Arabic gum and an extract from Okra *(Abelmoschus esculentus)* fruit, respectively. Then, the nanoparticles were characterized using UV-Vis, PL, FTIR, XRD, FESEM/TEM, and XPS techniques. The cytotoxicity, Annexin V-FITC apoptosis assay, and measurement of reactive oxygen species along with cellular uptake, were evaluated.

Results: The results of characterization confirmed the successful synthesis of SQDs and CeO_2 with a crystalline nature and the average size of 4.79 and 27.31 nm, respectively. The findings indicated that SQDs had no significant inhibitory effect on normal and cancer cells. The cell uptake of SQDs demonstrated high internalization into Y79 cells with an exited green light color under a fluorescent microscope. On the other hand, CeO_2 nanoparticles showed the ability to suppress the growth and increase early and late apoptosis of Y79 cells at concentrations of 500 µg/mL after 24 h. The level of reactive oxygen species (ROS) was also increased in Y79 cells after treatment with CeO_2.

Conclusion: As the SQDs exhibited green light color and CeO_2 enhanced apoptosis and ROS levels, this study suggested SQDs could be a potential bioimaging and labeling agent, while CeO_2 may be considered for therapeutic applications in retinoblastoma.

Introduction

Retinoblastoma is one of the most common ocular cancers in infants and young children (ages 1-3 years), with characteristic symptoms such as misaligned eyes (strabismus) and white pupils (leukocoria).[1,2] Depending on the stage of retinoblastoma, different treatment options are available, including photocoagulation, chemotherapy, cryotherapy, and surgery. Although these methods offer certain advantages, their clinical application is limited due to cytotoxicity, potential cataract formation, and

*Corresponding author: Afsane Bahrami, Emails: BahramiAF@mums.ac.ir; afsbahrami91@yahoo.com
#Equally contributed.

drug resistance.[3,4] Employing nanotechnology is a highly effective strategy to mitigate these adverse effects and enhance therapeutic efficacy. Various categories of nanomaterials, including nanoparticles, nanoliposomes, nanopolymers, and nanohydrogels, have been utilized in cancer treatment and diagnosis. These materials are particularly valuable due to their small size, high surface-to-volume ratio, diverse shapes, surface functionalization, and unique physicochemical properties.[5,6] Quantum dots (QDs) have been widely studied as imaging contrast agents and for in vivo cell monitoring. Their remarkable resistance to photobleaching, exceptional photoluminescence properties, and ultra-small size make them highly advantageous for these applications.[7,8] A dynamic study on QDs-labeled human corneal endothelial cell injection for imaging corneal endothelial dysfunctions demonstrated the quantitative aggregation of cells in both injured and non-injured eyes.[9] Although QDs have shown promising potential in ocular imaging, their substantial toxicity presents significant challenges. Consequently, metal-free quantum dots have emerged as viable alternatives to conventional QDs in biomedical applications. Notable examples include sulfur quantum dots (SQDs), carbon-based quantum dots, and phosphorus quantum dots. Among them, SQDs are particularly preferred due to their proven effectiveness as sensors and imaging probes, as well as their favorable biodistribution, antifungal, and antibacterial properties.[10-15] Moreover, metallic nanoparticles have demonstrated considerable promise in cancer therapy through both active and passive drug delivery mechanisms. Their ability to enhance treatment outcomes is further strengthened by their free radical scavenging activity and ability to induce apoptosis.[16,17] Among metallic nanoparticles, cerium oxide nanoparticles (CeO_2) exhibit great potential for anticancer, anti-inflammatory, and drug delivery applications.[18] Previous studies have shown that CeO_2 can protect normal cells at neutral pH through its antioxidant activity, owing to the presence of Ce^{3+} and Ce^{4+} oxidation states, which enable it to scavenge free radicals. However, in tumor environments, CeO_2 exhibits pro-oxidant properties, thereby inhibiting cancer cell growth.[17-19] Previous studies has also indicated that CeO_2 displays selective toxicity against retinoblastoma (Y79) and normal cells, with cytotoxic effects depending on the synthesis method.[20,21] In this study, we aimed to synthesize SQDs and CeO_2 for the first time using Arabic gum and okra (*Abelmoschus esculentus*) fruit extract, respectively. Green synthesis using plant-based methods is simple, non-toxic, and eco-friendly. Additionally, plant extracts serve as excellent capping agents and reducing agents by providing various bioactive compounds, including polyphenols, flavonoids, alkaloids, and organic acids.[22-24] Furthermore, Arabic gum is rich in hydroxyl groups, which can effectively stabilize SQDs.[25] This study aimed to synthesize and characterize SQDs and CeO_2 using various analytical techniques, explore the potential of SQDs as imaging probes, and assess the ROS-modulating effects of CeO_2 on Y79 cancer cells.

Materials and Methods

Chemicals and reagents

Dimethyl sulfoxide (DMSO), hydrogen peroxide (H_2O_2, 35%), penicillin/streptomycin, Sublimated sulfur powder (99%), Arabic gum, phosphate-buffered saline (PBS), resazurin and NaOH were purchased from Sigma Co (Burlington, Massachusetts, USA). Moreover, the fetal bovine serum (FBS) and the high glucose DMEM and RPMI 1640 were provided from GIBCO (Waltham, Massachusetts, USA). The $Ce(NO_3)_3.6H_2O$ salt was acquired from Merck Co (Darmstadt, Germany). The Abcam (Cambridge, United Kingdom) supplied the dichloro-dihydro-fluorescein diacetate (DCFDA)/ H2DCFDA-cellular ROS detection assay kit. All reagents used were of analytical grade and were utilized without further purification.

Biosynthesis of CeO_2

The green synthesis of CeO_2 nanoparticles began with the preparation of the plant extract. For this purpose, 20 g of fresh okra (*Abelmoschus esculentus*) fruit was washed, dried, and sliced into small pieces. The sliced okra was then added to 50 mL of distilled water, and the mixture was continuously stirred at 60 °C for 2 hours. After this period, the plant extract was obtained and subsequently filtered to remove any impurities.

In the next stage, CeO_2 nanoparticles were synthesized using the sol-gel method, with okra fruit extract acting as a capping and stabilizing agent. First, 4.37 g of $Ce(NO_3)_3{\cdot}6H_2O$ was dissolved in 50 mL of distilled water and stirred for 20 to 30 minutes at room temperature. Next, 10 mL of plant extract was added dropwise to the salt solution. The final mixture was stirred in an oil bath at 80 °C for 12 hours, resulting in the formation of a lemon-colored $Ce(OH)_2$ gel. This gel was then dried at 110 °C for 6 hours, followed by calcination at 400 °C for 2 hours, yielding yellow CeO_2 powder.[24,26]

Biosynthesis of SQDs

SQDs were synthesized using a one-pot hydrothermal method. Initially, 565 mg of Arabic gum was dispersed in 15 mL of H_2O_2 (10% v/v) under continuous stirring. Then, 20 mg of sublimated sulfur powder was added to the solution at room temperature. The mixture was homogenized using a sonicator bath for 2 minutes to ensure uniform dispersion. Next, the suspension was transferred to a Teflon-lined autoclave and heated to 220 °C for 24 hours, facilitating the hydrothermal reaction necessary for SQD formation. After the reaction, the solution was neutralized with 1.0 M NaOH to a pH of

7.0, and contaminants were removed using a 0.22 μm microporous filter.[27,28] For further analysis, the solution was freeze-dried and stored at 4 °C.

Characterization

To characterize the biosynthesized nanoparticles, several experimental techniques were employed. The absorbance band in the range of 200–800 nm was determined using UV-Vis spectroscopy (Shimadzu, Japan). The photoluminescence (PL) intensity of SQDs was measured using a fluorometer (Jasco, FP-6000 series, Germany).

Furthermore, FT-IR spectroscopy (Avatar 370, Thermo Nicolet, USA) was used to identify the functional groups present on the surface of the nanoparticles within the range of 400–4000 cm^{-1}. The crystalline structure of the biosynthesized SQDs and CeO_2 was analyzed using X-ray diffraction (XRD), while the purity, morphology, and size of the samples were evaluated using field emission scanning electron microscopy (FESEM) (TESKAN MIRA 3, Czech Republic) and transmission electron microscopy (TEM) (Zeiss, EM10C, Germany). Additionally, the elemental composition of the synthesized nanoparticles was determined using X-ray photoelectron spectroscopy (XPS) (ESCALab220I-XL, VG Scientific, Canada), a quantitative technique for surface analysis.

Evaluation of the cytotoxic activity of nanoparticles

The retinoblastoma cell line (Y79) and human foreskin fibroblast (HFF) cells were purchased from the Pasteur Institute (Tehran, Iran). These cells were incubated in RPMI 1640 and high-glucose DMEM media, supplemented with 10% FBS and 1% penicillin/streptomycin, at 37 °C until they reached sufficient confluency.

To assess the cytotoxicity of the nanoparticles, Y79 and HFF cells were seeded in a 96-well plate at a density of 2×10^4 cells per well and incubated overnight. The next day, the cells were treated with varying concentrations of SQDs (0–1000 μg/mL) and CeO_2 (0–1000 μg/mL) for 24 hours.

Following incubation, 20 μL of resazurin was added to each well, and the plates were gently shaken before being incubated for an additional 3 hours. During this period, living cells converted resazurin into resorufin. The fluorescence of resorufin was measured using a VICTOR X5 Multimode Plate Reader (Perkin-Elmer, Waltham, MA, USA) by exciting the sample at 530 nm and detecting emission at 590 nm. Each experiment was performed in triplicate, and the results were reported as mean ± SD.[29]

Measurement of ROS activity

Following the manufacturer's instructions, the cellular ROS detection kit was used to determine the ROS levels. Y79 and HFF cells were seeded in 96-well plates at a density of 25×10^3 cells per well and incubated overnight. The cells were then washed and stained with 20 μM H_2DCFDA solution for 45 minutes in the dark. After staining, the cells were rewashed and exposed to 250 μg/mL and 500 μg/mL of CeO_2 for 8 hours. The fluorescence intensity was measured using a VICTOR X5 Multimode Plate Reader with a filter set (Excitation/Emission: 485/535 nm). A positive control, 150 μM of tert-butyl hydroperoxide (TBHP), was used for comparison.

Annexin V-FITC assay

The Annexin V-FITC/PI assay was performed to evaluate the rate of Y79 cell apoptosis and necrosis following treatment with 500 μg/mL of CeO_2 and SQDs according to manufacture instruction (Cayman Chemical, Michigan, MI, USA). In summary, 10^5 cells were cultured in DMEM supplemented with 10% FBS. After a 24-hour incubation, the cells were treated with 500 μg/mL of CeO_2 and SQDs for an additional 24 hours. The treated cells were then collected and rinsed with incubation buffer. Subsequently, the cells were stained with Annexin V-FITC/PI and analyzed using a BD FACSCalibur™ Flow Cytometer (Becton Dickinson, USA).

Cell uptake of SQDs

The cell uptake experiment was performed using Y79 cell lines. Briefly, 1.5×10^5 cells were cultured for 24 hours at 37 °C in 12-well plates. SQDs (500 μg/mL) were then added to each well and incubated for an additional 4 hours. Afterward, the media was centrifuged, and the supernatant was separated to remove any unattached SQDs. Finally, the internalization was observed using a fluorescent microscope (Axiovert 200, Zeiss, Germany).

Furthermore, internalization of SQDs was evaluated using flow cytometry in both untreated control cells and Y79 cells treated with SQDs at a concentration of 500 μg/mL. After treatment of cells for 4 hours, cells were washed with PBS and 10 000 of cells were evaluated using a BD FACSCalibur™ Flow Cytometer (Becton Dickinson, USA).

Statistical Analysis

The statistical analysis was performed using the GraphPad Prism software. A P value of < 0.05 was considered significant. Data analysis was conducted using the Kruskal-Wallis test, one-way ANOVA, and Dunn's test for pairwise comparisons. Data are presented as mean ± standard deviation (SD).

Results

UV–Vis and PL analyses

UV-Vis analysis was performed to determine the maximum absorbance band of SQDs and CeO_2 in the 200–800 nm range (Fig. 1). According to the figure, the absorption band at 237.5 nm in the UV-Vis spectra of SQDs is attributed to the S_8^{2-} species. Moreover, the maximum absorbance for CeO_2 was observed at 305 nm, which is associated with charge transfer from the 2P (O) to

4f (Ce) orbitals. The PL emission spectra of SQDs, under excitation from 280 to 410 nm, exhibited excitation-dependent emission due to quantum confinement effects (Fig. 2c). The highest emission intensity was observed at 412 nm under an excitation wavelength of 350 nm.

FT-IR analysis

The FT-IR spectra of SQDs and CeO_2 nanoparticles are shown in Fig. 2. The surface functional groups of the nanoparticles were identified using FTIR analysis. The findings indicated that the –OH stretching vibration of H_2O adsorbed on the surface of the nanoparticles corresponds to the characteristic bands in the 3300 to 3500 cm^{-1} range. The stretching modes of the C=C, C–N, and C–O–C groups, associated with other organic molecules, are located approximately in the ranges of 1500 cm^{-1}, 1300 cm^{-1}, and 1100 cm^{-1}, respectively.[35]

In addition, the characteristic peak in the FTIR spectrum

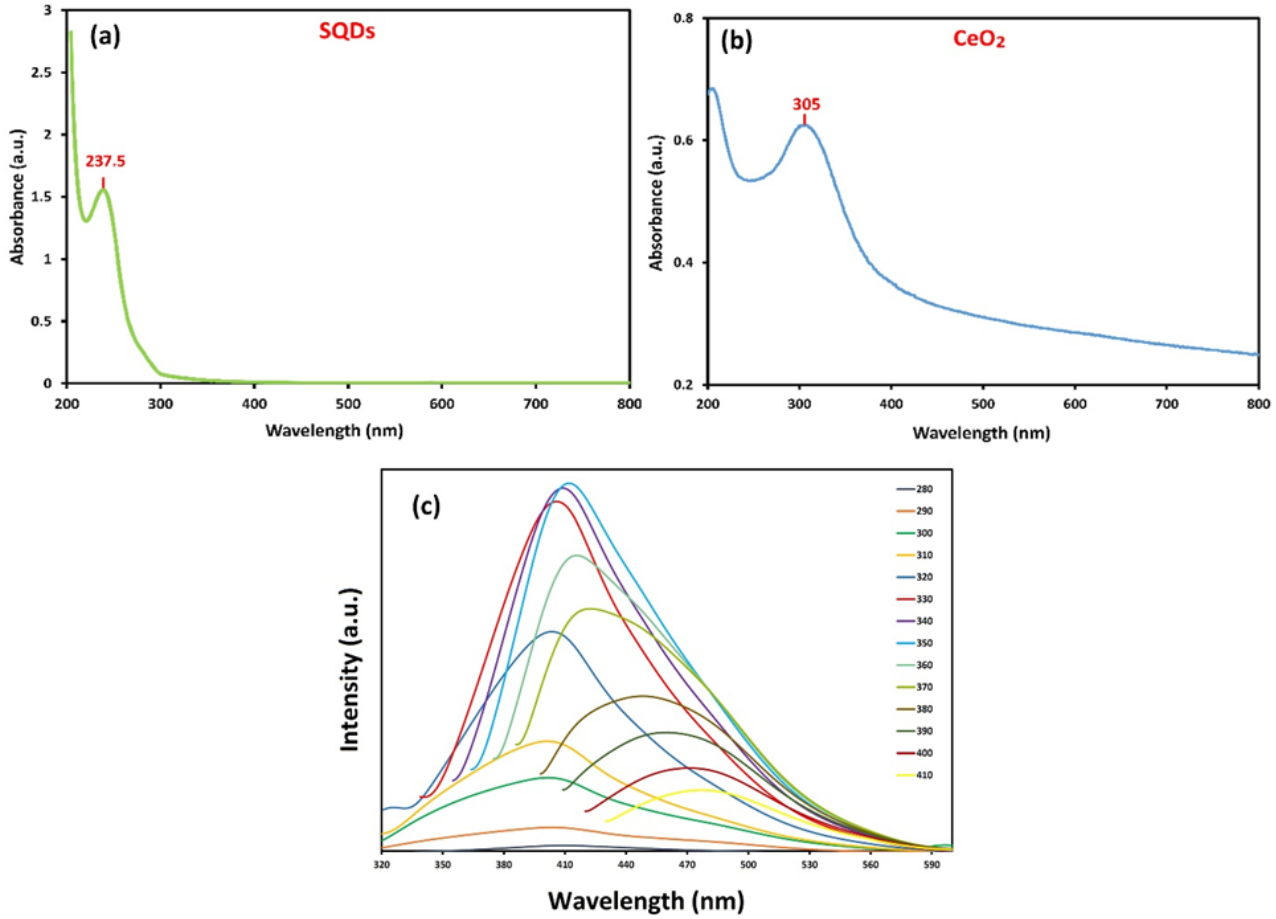

Fig. 1. The UV–Vis spectra of the synthesized SQDs (a), CeO_2 (b), and the PL spectra of the SQDs (c).

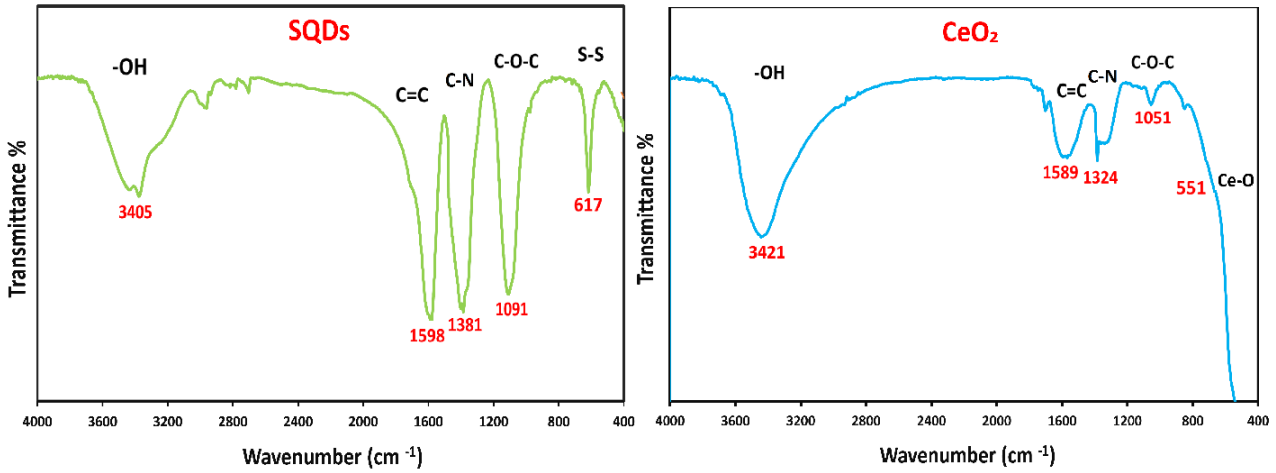

Fig. 2. FT-IR spectra of the synthesized SQDs and CeO_2 nanoparticles.

of SQDs is a band at a low energy, around 617 cm^{-1}, which is related to the presence of the S-S group. Moreover, the distinctive band at 551 cm^{-1} in the FTIR spectrum of CeO_2 corresponds to the stretching vibration of Ce–O. These absorption peaks confirm the successful synthesis of green-synthesized SQDs and CeO_2 nanoparticles.

XRD pattern

The XRD patterns of SQDs and CeO_2 nanoparticles are shown in Fig. 3. The XRD technique can be used to investigate the crystallographic structure and chemical composition of materials. According to the XRD diagram of SQDs, the different index values of (113), (202), (026), (206), (313), (044), and (317) planes are observed at 2θ values of 11°, 21°, 26°, 30°, 33°, 39°, and 45°, respectively. These results match with JCPDS #01-074-2109.[32]

In addition, the XRD pattern of CeO_2 displayed a face-centered cubic (fcc) crystalline structure without any impurities. The different index values of (111), (200), (220), (311), (222), (400), (331), and (420) planes are represented at 2θ values of 28°, 33°, 47°, 56°, 59°, 70°, 76°, and 78°, respectively, which match with JCPDS #00-034-0394. A high level of purity is indicated by the XRD pattern, revealing no possible $Ce(OH)_3$/$Ce(OH)_4$ phases.

FESEM and TEM images

The FESEM images of SQDs and CeO_2 nanoparticles are presented in Fig. 4. The morphology and particle-size analysis (PSA) of the nanoparticles were assessed using FESEM images. The FESEM image of SQDs revealed a sphere-like shape with nanoscale diameters, while CeO_2 nanoparticles appeared homogeneous and nearly spherical. Additionally, the PSA of SQDs and CeO_2 nanoparticles were approximately 15.05 nm and 27.31 nm, respectively (Fig. 4).[38]

To obtain a more accurate size of SQDs, a TEM image was captured. The obtained image indicated that the spherical morphology of SQDs had a mean size of around 4.79 nm (Fig. 4E). It is worth noting that the size of SQDs in the FESEM images appears slightly larger than in the TEM images because FESEM captures images from the surface in three dimensions.

XPS analysis

The XPS scans of SQDs and CeO_2 nanoparticles are presented in Fig. 5. XPS analysis is used to detect surface elements of nanoparticles. For SQDs, the high-resolution S 2p spectrum shows peaks at 170, 168, and 166 eV, which indicate that the surface of SQDs contains SO_3^{2-} ($2p^{1/2}$), SO_2^{2-} ($2p^{3/2}$), and zero-valent sulfur, which is similar to previous reports.[39] Additionally, the high-resolution spectrum of CeO_2 presented Ce 3d, which corresponds to a relatively higher abundance of Ce^{4+} and Ce^{3+}. The binding energy peaks at 917.2, 898.7, 883.2, and 889.6 eV are related to Ce^{4+}, while the peaks at 906.5, 900, and 886 eV are attributed to Ce^{3+}.[40,41] XPS analysis revealed that the synthesized CeO_2 had a higher proportion of Ce^{4+} than Ce^{3+}.

Cytotoxicity evaluation

The antiproliferative effect of the biosynthesized nanoparticles was evaluated on Y79 and HFF cells. The resazurin assay, which measures cell viability by converting resazurin into resorufin, was used in this study. For SQDs, no significant inhibitory effect was observed on either Y79 or HFF cells. The results indicate that SQDs are highly biocompatible, exhibiting minimal toxicity toward both normal and tumor cells (Fig. 6B). In contrast, CeO_2 nanoparticles showed a concentration-dependent cytotoxic effect. Y79 and HFF cells were treated with varying concentrations of CeO_2 (0–1000 µg/mL) for 24 h. As shown in Fig. 6A, CeO_2 significantly inhibited the growth of Y79 cells at 500 µg/mL. Moreover, at 500 and 1000 µg/mL, CeO_2 exerted a notable cytotoxic effect on Y79 cells compared to the control group. However, CeO_2 did not induce any significant toxicity in normal HFF cells within 24 h (Fig. 6A).

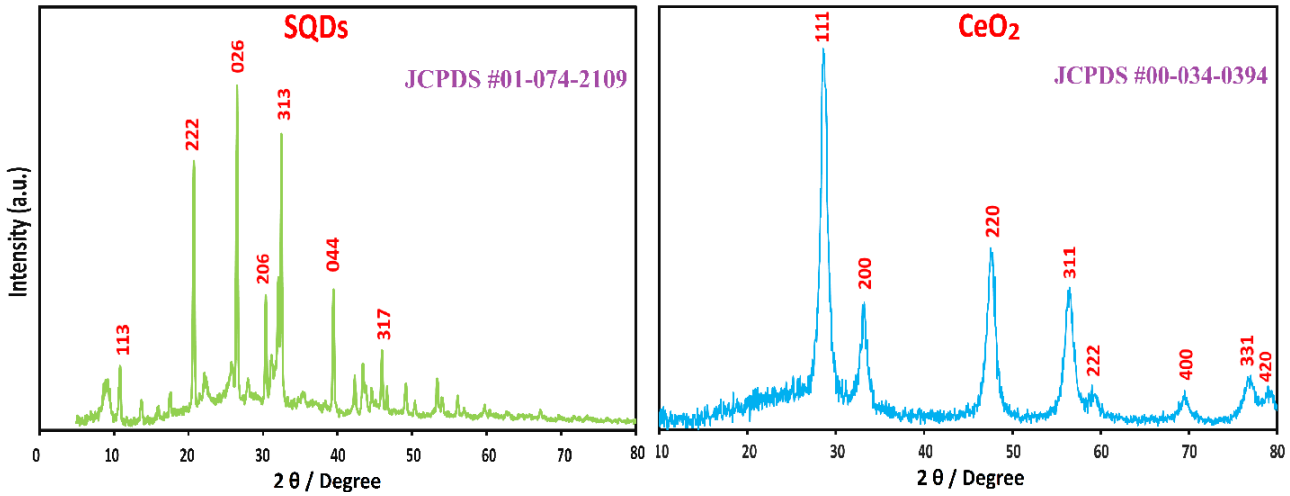

Fig. 3. XRD patterns of the synthesized SQDs and CeO_2 nanoparticles.

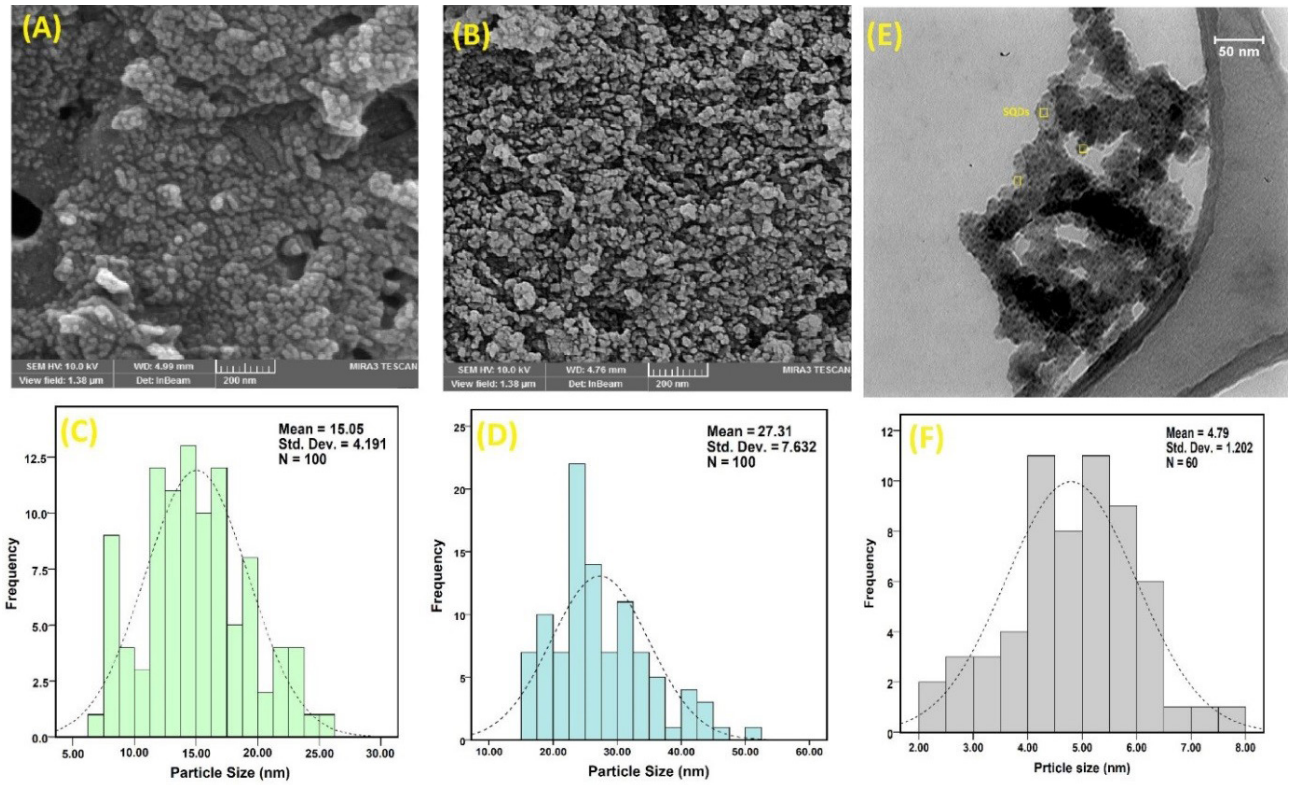

Fig. 4. FESEM/ PSA images of synthesized SQDs (A, C), CeO2 (B, D), and TEM/PSA images of SQDs (E, F).

ROS activity of CeO_2

The cellular ROS detection kit was used to assess the effect of CeO_2 nanoparticles on reactive oxygen species (ROS) generation. As shown in Fig. 6C, HFF cells treated with CeO_2 exhibited no significant change in ROS levels compared to the control group. However, in Y79 cells, ROS levels increased significantly at 500 µg/mL relative to the control. These findings suggest that CeO_2 nanoparticles can elevate ROS levels in retinoblastoma cells while exerting a protective effect in human foreskin fibroblast cells.

Apoptosis and necrosis of Y79 cells

Apoptosis and necrosis of CeO_2 and SQD-treated Y79 cells were analyzed using flow cytometry. The results indicated a significant increase in the rate of early and late apoptotic cells following treatment with CeO_2, reaching 63.7%, compared to 1.45% in the control group. In contrast, SQDs did not induce a notable increase in apoptosis, with only 2.86% of cells undergoing early or late apoptosis, compared to 1.45% in the control (Fig. 6D).

Cell uptake of SQDs

Due to their ultra-small size, photoluminescence (PL) emission, surface functional groups, and biocompatibility, SQDs hold significant potential for cell imaging, targeted imaging, and diagnostic applications. To assess their suitability, the cytotoxicity of SQDs was evaluated against Y79 and HFF cells, demonstrating very low toxicity. Subsequently, the cellular uptake efficiency was analyzed using fluorescence microscopy. As shown in Fig. 7A, SQDs emitted a green fluorescence under blue light excitation and exhibited high penetration into cancer cells after 4 hours, consistent with previous reports.[14,42] The observed low fluorescence intensity was due to the limitations of the fluorescence microscope, which only had two excitation wavelengths, preventing adjustment to the maximum emission wavelength. Additionally, we evaluate the amount of cellular uptake using flow cytometry. As shown in Figs. 7C and 7D, 97.3% of the cells were positive for SQDs uptake following treatment with SQDs. These findings suggest that SQDs could be considered as a promising candidates for bioimaging and diagnostic applications.

Discussion

Retinoblastoma is a pediatric ocular cancer that affects the retina, the light-sensitive tissue at the back of the eye. It is the most common intraocular malignancy in children, typically developing before the age of five.[43] Traditional treatments, including enucleation, chemotherapy, and radiotherapy, often lead to significant side effects and may not always preserve vision.

In this context, nanotechnology offers promising advancements in retinoblastoma treatment.[44,45] Nanoparticles can be engineered for targeted drug delivery, improving treatment efficacy while reducing systemic side effects. This study investigates the potential of SQDs and

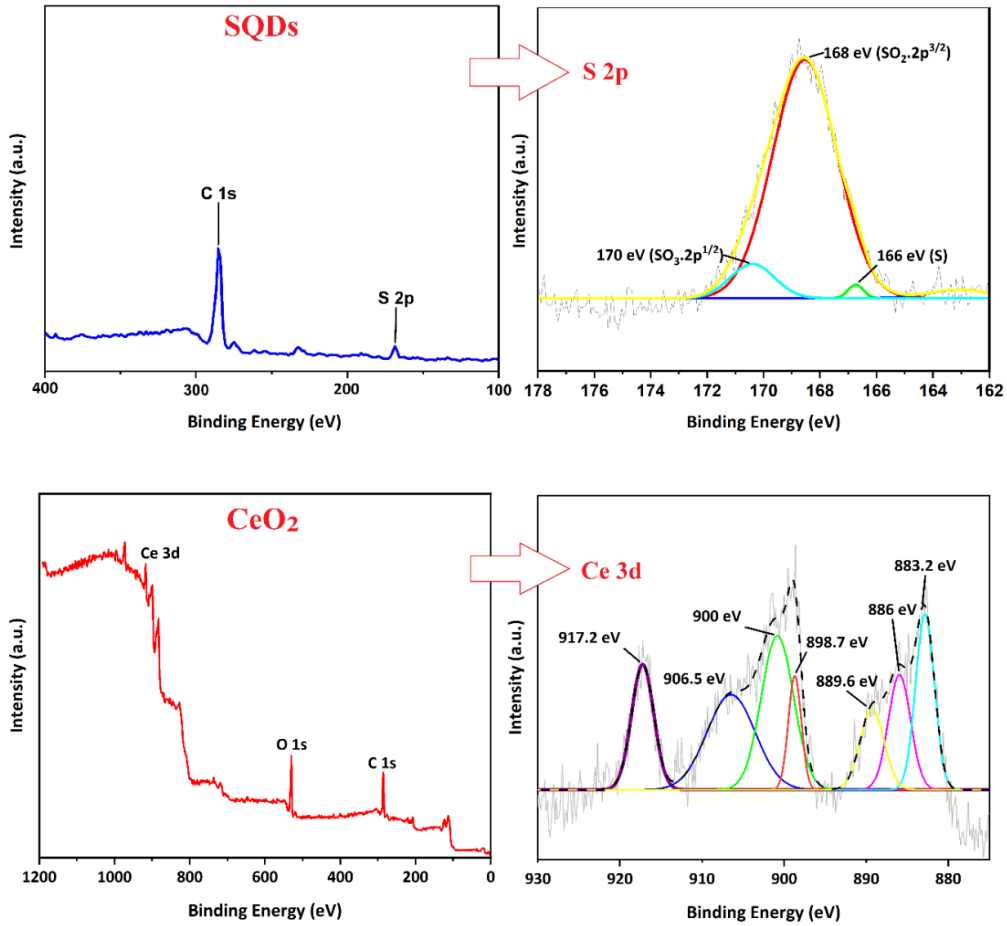

Fig. 5. XPS spectrum of the synthesized SQDs and CeO_2 nanoparticles

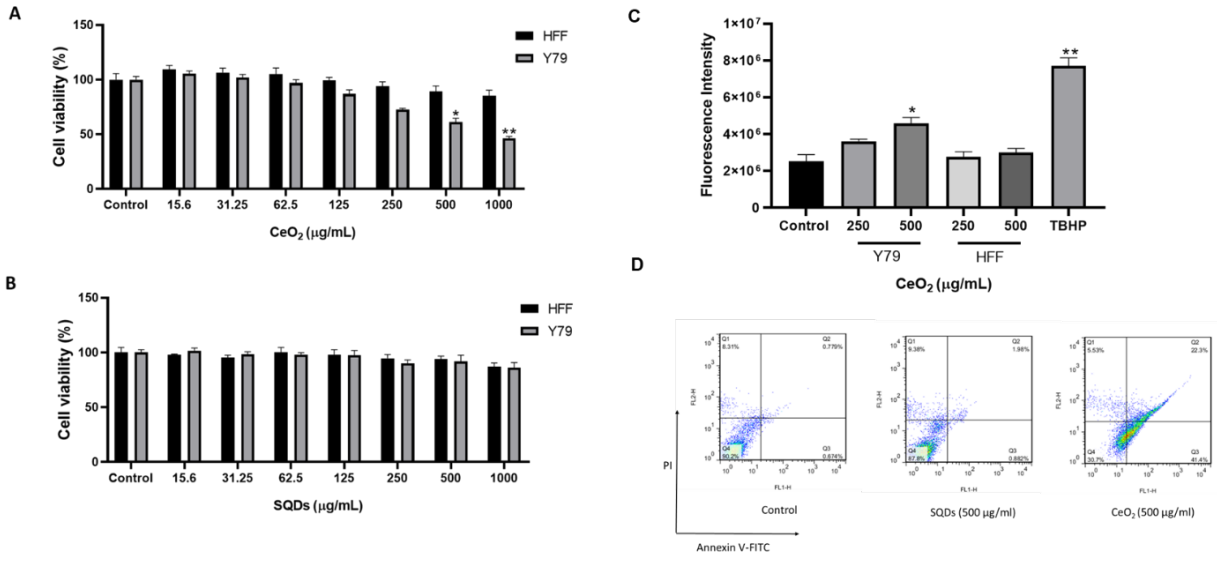

Fig. 6. The cytotoxicity effects of CeO_2 **(A)** and SQDs **(B)** nanoparticles on cancer cells (Y79) and normal cells (HFF) compared to the control group over 24 h. Both cell types were incubated with varying concentrations of CeO_2 and SQDs for 24 h. The cell viability was assessed using the resazurin assay. **(C)** The effects of CeO_2 on the reactive oxygen species (ROS) levels of Y79 and HFF cells compared to the control group. Our data demonstrate that CeO_2 nanoparticles induced an increase in ROS levels of Y79 cells within 24 h, while there was no significant change in HFF cells. In the positive control sample treated with tert-butyl hydroperoxide (TBHP) at a concentration of 150 μM, the fluorescence intensity was significantly elevated compared to the control group. The data are presented as mean ± standard deviation (SD) for at least 3 replicates for each experimental point (∗p < 0:05, ∗∗p < 0:01 as compared with the control). **(D)** The apoptosis evaluation of 500 μg/mL of CeO_2 and SQDs nanoparticles on Y79 cells compared to the control group over 24 h. A markedly higher amount of early and late apoptosis was detected in CeO2 treated Y79 cells vs. control. Q4 to Q1 of the diagram represent live cells, early apoptotic, late apoptotic, and necrotic cells, respectively. PI: Propidium iodide.

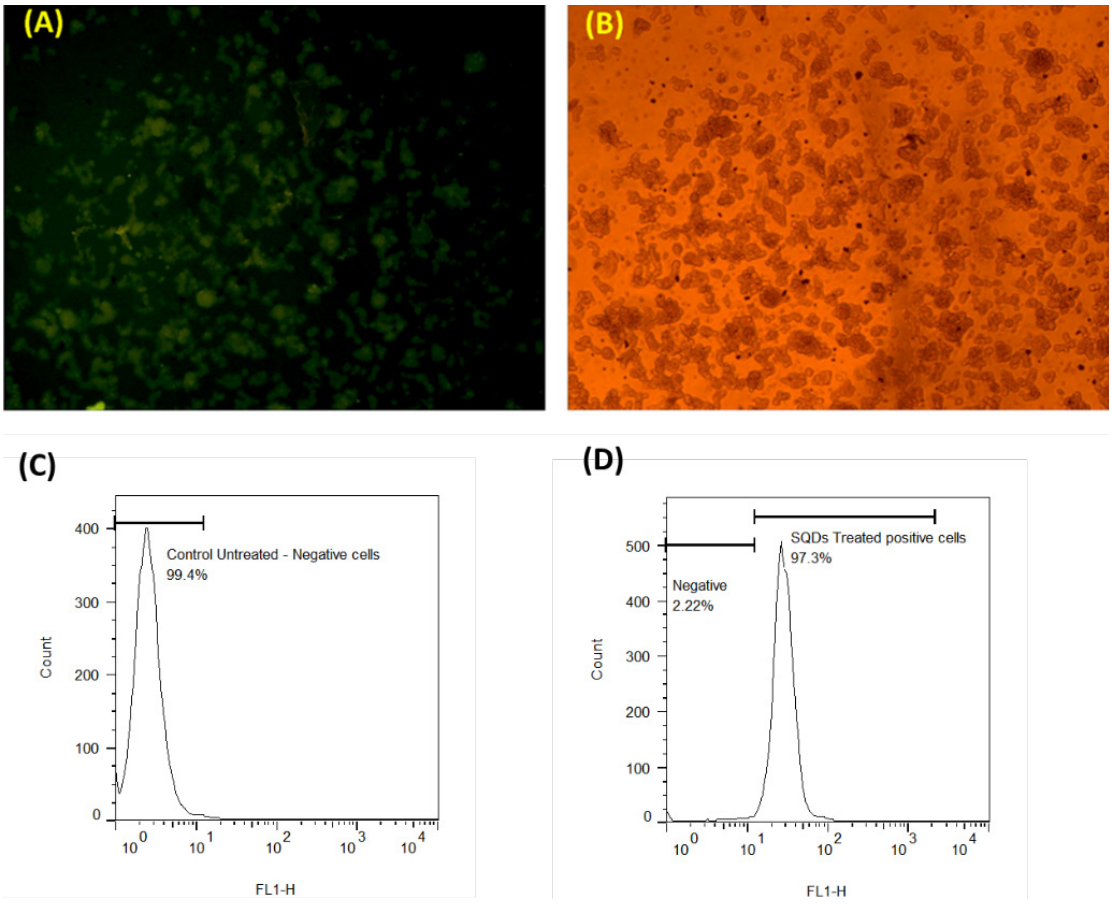

Fig. 7. The microscopic images of cell uptake of SQDs, **(A)** (fluorescence microscope) and **(B)** (Bright-field microscope). The retinoblastoma Y79 cells were treated with 500 µg/mL of SQDs for a duration of 4 h. Excited green light color indicates the successful internalization of quantum dots within the cancer cells. Evaluating the internalization of SQDs using flow cytometry, comparing the **(C)** untreated Y79 cells with **(D)** cells treated with SQDs (500 µg/mL) for 4 hours.

CeO_2 due to their unique properties. Characterization analyses confirmed that both nanoparticles were synthesized at the nanoscale and exhibited spherical morphologies. SQDs typically range from 2 to 10 nm, with TEM imaging revealing an average size of 4.79 nm, making them highly suitable for cancer cell internalization. Their small size is critical for enhanced photoluminescence and stability.[46,47] Furthermore, XRD analysis verified the high purity and crystalline structure of both SQDs and CeO_2, aligning with previous studies.[28,48]

The distinct peaks observed in the XRD patterns align with standard JCPDS values, confirming well-defined crystallographic phases with no detectable impurities. The XPS analysis of SQDs revealed binding energy peaks at 170, 168, and 166 eV, corresponding to the oxidized sulfur composition of SO_3^{2-} ($2p^{1/2}$), SO_2^{2-} ($2p^{3/2}$), and zero-valent. Liu et al demonstrated that the formation of divalent sulfur ions and SO_3^{2-} results from the reaction between NaOH and bulk sulfur.[49] Additionally, the XPS spectrum of CeO_2 confirmed the presence of the Ce^{3+}/Ce^{4+} redox couple, consistent with previous studies that reported similar binding energy values for Ce^{4+} and Ce^{3+}.[50] In this context, Gupta et al reported that a higher Ce^{3+} content enhances superoxide dismutase (SOD) mimetic activity, while a higher Ce^{4+} state can lead to increased catalytic activity and potential pro-oxidant effects.[51] The cytotoxicity evaluation using the resazurin assay revealed distinct outcomes for SQDs and CeO_2 nanoparticles. SQDs exhibited high biocompatibility and extremely low toxicity toward both normal and tumor cells. In our previous study, SQDs demonstrated minimal cytotoxicity in both cancer (C26) and normal (L929) cell lines, making them suitable probes for cellular labeling and imaging.[32] In contrast, the synthesized CeO_2 nanoparticles significantly inhibited the growth of Y79 cells at a concentration of 500 µg/mL. Similarly, a study by Nazaripour et al reported that CeO_2 nanoparticles synthesized using *Prosopis farcta* fruit extract exhibited approximately 58% cytotoxic activity against colon cancer (HT-29) cells at 500 µg/mL.[52] To assess the impact of CeO_2 nanoparticles on ROS generation, the cellular ROS detection kit was employed. The findings indicate that CeO_2 nanoparticles exhibit pro-oxidant activity and induce ROS production in retinoblastoma (Y79) cells, while simultaneously demonstrating antioxidant properties in normal cells. This dual effect of CeO_2 on ROS generation has been linked to the pH-dependent behavior of the nanoparticles. Studies have established that CeO_2 exhibits antioxidant activity at

physiological pH, acting as a cellular protector, but shifts to an oxidase-like activity in acidic environments, such as the tumor microenvironment.[53-55]

Moreover, CeO_2 nanoparticles with a higher Ce^{3+} content (~62%) have been reported to exhibit notable antioxidant activity, reducing ROS levels in A2780 ovarian cancer cells. Conversely, a CeO_2 formulation with lower Ce^{3+} content (~24%) has been shown to enhance ROS generation, highlighting the oxidation-state-dependent properties of the nanoparticles.[56,57] Our study confirms that the synthesized CeO_2 nanoparticles contain a higher proportion of Ce^{4+} states relative to Ce^{3+}, which suggests their potential to induce pro-oxidant activity and cytotoxicity in retinoblastoma cells.

Furthermore, the cellular uptake analysis of SQDs demonstrated that after 4 hours, the quantum dots successfully penetrated Y79 cells. Research suggests that SQDs are promising fluorescent agents for bioimaging applications due to their high colloidal stability, stable optical properties, low toxicity, and bioavailability.[58] Consistent with our findings, Song et al utilized fluorescent SQDs (20 µg/mL) to stain MCF-7 breast cancer cells for 2 hours. Upon excitation at 458 nm and 514 nm, strong green and yellow emissions were observed in the cytoplasm, indicating efficient SQD internalization.[59] Additionally, Qiao et al demonstrated that after an 8-hour incubation, SQDs accumulated in the cytoplasm of HeLa and K562 leukemia cells, with uptake occurring primarily via clathrin-mediated and lipid-raft-mediated endocytosis.[38] These studies, alongside our findings, reinforce the potential of SQDs for advanced cellular imaging applications.

Conclusion

In this study, SQDs and CeO_2 nanoparticles were synthesized using Arabic gum and okra (*Abelmoschus esculentus*) fruit extract via an environmentally friendly, non-toxic, cost-effective, and rapid method. Various characterization techniques were employed to analyze the morphology and structure of the synthesized nanoparticles. The results confirmed the successful synthesis of both SQDs and CeO_2 nanoparticles, exhibiting spherical-like shapes with nanoscale dimensions. Cytotoxicity evaluation using the resazurin assay demonstrated that SQDs exhibited low toxicity toward both normal and cancer cells, suggesting their biocompatibility. In contrast, CeO_2 nanoparticles significantly inhibited the proliferation of Y79 retinoblastoma cells at a concentration of 500 µg/mL, while exhibiting minimal toxicity toward normal cells. Furthermore, cellular uptake analysis confirmed that SQDs effectively penetrated cancer cells, highlighting their potential as fluorescent probes for cancer diagnosis and biomedical imaging. Additionally, the findings suggest that CeO_2 nanoparticles hold promise as a viable anti-tumor agent, as they selectively suppress cancer cell growth without causing damage to normal tissues.

Acknowledgements

We would like to thank the Clinical Research Development Unit, Imam Reza Hospital, Mashhad University of Medical Sciences, for their assistance in this manuscript.

Authors' Contribution

Conceptualization: Zahra Foroutan, Sadaf Afshari.
Data curation: Sajjad Njafi, Amir R. Afshari, Seyed Sajad Ahmadi, Seyedsina Nemati, Seyedeh Mozhdeh Mirzaei.
Formal analysis: Zahra Foroutan, Sadaf Afshari.
Funding acquisition: Afsane Bahrami.
Investigation: Zahra Foroutan, Sadaf Afshari, Sajjad Njafi, Amir R. Afshari, Seyed Sajad Ahmadi, Seyedsina Nemati, Seyedeh Mozhdeh Mirzaei.
Methodology: Zahra Foroutan, Sadaf Afshari.
Project administration: Afsane Bahrami.
Resources: Afsane Bahrami.
Supervision: Afsane Bahrami.
Validation: Sajjad Njafi, Amir R. Afshari, Seyed Sajad Ahmadi, Seyedsina Nemati, Seyedeh Mozhdeh Mirzaei.
Visualization: Afsane Bahrami.
Writing-original draft: Zahra Foroutan, Sadaf Afshari.
Writing-review & editing: Sajjad Njafi, Amir R. Afshari, Seyed Sajad Ahmadi, Seyedsina Nemati, Seyedeh Mozhdeh Mirzaei.

Competing Interests

The authors declare that there is no conflict of interest.

Ethical Approval

The project was found to be in accordance to the ethical principles and

Research Highlights

What is the current knowledge?

- Retinoblastoma is a common childhood ocular cancer, typically presenting with symptoms like strabismus and leukocoria.
- Conventional treatments (chemotherapy, photocoagulation) are limited by side effects, including cytotoxicity and drug resistance.
- Nanotechnology, including quantum dots and nanoparticles, has shown potential for targeted cancer therapies and imaging.

What is new here?

- This study presents the first synthesis of SQDs and CeO2 nanoparticles using Arabic gum and okra extract as eco-friendly agents.
- SQDs demonstrated low toxicity towards both Y79 retinoblastoma cells and normal cells, indicating their high biocompatibility and potential as imaging probes.
- Cerium oxide nanoparticles selectively inhibited Y79 cancer cell proliferation and increase apoptosis while providing protection to normal cells via reactive oxygen species modulation, showcasing their dual role in cancer therapy.
- The synthesis and characterization of SQDs and CeO2 nanoparticles provide insights into their structural properties, enhancing the understanding of their application in retinoblastoma treatment and imaging diagnostics.

the national norms and standards for conducting Medical Research in Iran (Approval No. IR.MUMS.IRH.REC.1403.038).

Funding

This study supported by Mashhad University of Medical Sciences (grant number: 4022444).

References

1. Fabian ID, Onadim Z, Karaa E, Duncan C, Chowdhury T, Scheimberg I, et al. The management of retinoblastoma. *Oncogene* **2018**; 37: 1551-60. doi: 10.1038/s41388-017-0050-x.
2. Balmer A, Munier F. Differential diagnosis of leukocoria and strabismus, first presenting signs of retinoblastoma. *Clin Ophthalmol* **2007**; 1: 431-9.
3. Arshad R, Barani M, Rahdar A, Sargazi S, Cucchiarini M, Pandey S, et al. Multi-functionalized nanomaterials and nanoparticles for diagnosis and treatment of retinoblastoma. *Biosensors (Basel)* **2021**; 11: 97. doi: 10.3390/bios11040097.
4. Shields CL, Shields JA, De Potter P, Minelli S, Hernandez C, Brady LW, et al. Plaque radiotherapy in the management of retinoblastoma. Use as a primary and secondary treatment. *Ophthalmology* **1993**; 100: 216-24. doi: 10.1016/s0161-6420(93)31667-2.
5. Mandal M, Banerjee I, Mandal M. Nanoparticle-mediated gene therapy as a novel strategy for the treatment of retinoblastoma. *Colloids Surf B Biointerfaces* **2022**; 220: 112899. doi: 10.1016/j.colsurfb.2022.112899.
6. Sanati M, Afshari AR, Simental-Mendía LE, Sahebkar A. Nanohybrid drug delivery approach as a novel opportunity for curcumin delivery in cancer. In: Kesharwani P, Sahebkar A, eds. *Curcumin-Based Nanomedicines as Cancer Therapeutics*. Academic Press; **2024**. p. 339-53. doi: 10.1016/b978-0-443-15412-6.00019-2.
7. Garner I, Vichare R, Paulson R, Appavu R, Panguluri SK, Tzekov R, et al. Carbon dots fabrication: ocular imaging and therapeutic potential. *Front Bioeng Biotechnol* **2020**; 8: 573407. doi: 10.3389/fbioe.2020.573407.
8. Abdellatif AA, Younis MA, Alsharidah M, Al Rugaie O, Tawfeek HM. Biomedical applications of quantum dots: overview, challenges, and clinical potential. *Int J Nanomedicine* **2022**; 17: 1951-70. doi: 10.2147/ijn.S357980.
9. Toda M, Yukawa H, Yamada J, Ueno M, Kinoshita S, Baba Y, et al. In vivo fluorescence visualization of anterior chamber injected human corneal endothelial cells labeled with quantum dots. *Invest Ophthalmol Vis Sci* **2019**; 60: 4008-20. doi: 10.1167/iovs.19-27788.
10. Ruan H, Zhou L. Synthesis of fluorescent sulfur quantum dots for bioimaging and biosensing. *Front Bioeng Biotechnol* **2022**; 10: 909727. doi: 10.3389/fbioe.2022.909727.
11. Mohkam M, Sadraeian M, Lauto A, Gholami A, Nabavizadeh SH, Esmaeilzadeh H, et al. Exploring the potential and safety of quantum dots in allergy diagnostics. *Microsyst Nanoeng* **2023**; 9: 145.
12. Kumar JV, Tammina SK, Rhim JW. One-step hydrothermal synthesis of sulfur quantum dots for detection of Hg2 + ions and latent fingerprints. *Colloids Surf A Physicochem Eng Asp* **2024**; 690: 133682. doi: 10.1016/j.colsurfa.2024.133682.
13. Mirzaei SM, Sabouri Z, Kazemi Oskuee R, Sadri K, Farasati Far B, Darroudi M. A highly selective fluorescent biosensor based on sulfur quantum dots for iron (III) detection. *Mater Today Commun* **2024**; 38: 108131. doi: 10.1016/j.mtcomm.2024.108131.
14. Arshad F, Sk MP, Maurya SK, Siddique HR. Mechanochemical synthesis of sulfur quantum dots for cellular imaging. *ACS Appl Nano Mater* **2021**; 4: 3339-44. doi: 10.1021/acsanm.1c00509.
15. Tammina SK, Priyadarshi R, Rhim JW. Dual functions of metal ion detection and antibacterial activity of sulfur quantum dots. *New J Chem* **2023**; 47: 7733-45. doi: 10.1039/d3nj00373f.
16. Remya RR, Rajasree SR, Suman TY, Aranganathan L, Gayathri S, Gobalakrishnan M, et al. Laminarin based AgNPs using brown seaweed *Turbinaria ornata* and its induction of apoptosis in human retinoblastoma Y79 cancer cell lines. *Mater Res Express* **2018**; 5: 035403. doi: 10.1088/2053-1591/aab2d8.
17. Foroutan Z, Afshari AR, Sabouri Z, Mostafapour A, Farasati Far B, Jalili-Nik M, et al. Plant-based synthesis of cerium oxide nanoparticles as a drug delivery system in improving the anticancer effects of free temozolomide in glioblastoma (U87) cells. *Ceram Int* **2022**; 48: 30441-50. doi: 10.1016/j.ceramint.2022.06.322.
18. Nourmohammadi E, Khoshdel-Sarkarizi H, Nedaeinia R, Darroudi M, Kazemi Oskuee R. Cerium oxide nanoparticles: a promising tool for the treatment of fibrosarcoma in-vivo. *Mater Sci Eng C Mater Biol Appl* **2020**; 109: 110533. doi: 10.1016/j.msec.2019.110533.
19. Wason MS, Zhao J. Cerium oxide nanoparticles: potential applications for cancer and other diseases. *Am J Transl Res* **2013**; 5: 126-31.
20. Kartha B, Thanikachalam K, Vijayakumar N, Alharbi NS, Kadaikunnan S, Khaled JM, et al. Synthesis and characterization of Ce-doped TiO2 nanoparticles and their enhanced anticancer activity in Y79 retinoblastoma cancer cells. *Green Process Synth* **2022**; 11: 143-9. doi: 10.1515/gps-2022-0011.
21. Gao R, Mitra RN, Zheng M, Wang K, Dahringer JC, Han Z. Developing nanoceria-based pH-dependent cancer-directed drug delivery system for retinoblastoma. *Adv Funct Mater* **2018**; 28: 1806248. doi: 10.1002/adfm.201806248.
22. Taghavizadeh Yazdi ME, Amiri MS, Hosseini HA, Kazemi Oskuee R, Mousavi SH, Pakravanan K, et al. Plant-based synthesis of silver nanoparticles in *Handelia trichophylla* and their biological activities. *Bull Mater Sci* **2019**; 42: 155. doi: 10.1007/s12034-019-1855-8.
23. Osman AI, Zhang Y, Farghali M, Rashwan AK, Eltaweil AS, Abd El-Monaem EM, et al. Synthesis of green nanoparticles for energy, biomedical, environmental, agricultural, and food applications: a review. *Environ Chem Lett* **2024**; 22: 841-87. doi: 10.1007/s10311-023-01682-3.
24. Foroutan Z, Sabouri Z, Afshari AR, Mostafapour A, Farasati Far B, Jalili-Nik M, et al. Green synthesis of cerium oxide nanoparticles via *Linum usitatissimum* seeds extract and assessment of its biological effects. *Micro Nano Lett* **2024**; 19: e270003. doi: 10.1049/mna2.70003.
25. Farooq M, Sagbas S, Yildiz M, Meral K, Siddiq M, Aktas N, et al. Gum Arabic microgels as template for in situ metal-sulfide based quantum dots preparation and their thermal, spectroscopic, optical, and magnetic characterization. *J Electron Mater* **2017**; 46: 4373-83. doi: 10.1007/s11664-017-5394-z.
26. Sabouri Z, Mohammad S, Sadegh AM, Mehrdad K, Darroudi M. Plant-based synthesis of cerium oxide nanoparticles using *Rheum turkestanicum* extract and evaluation of their cytotoxicity and photocatalytic properties. *Mater Technol* **2022**; 37: 555-68. doi: 10.1080/10667857.2020.1863573.
27. Gallardo-Benavente C, Carrión O, Todd JD, Pieretti JC, Seabra AB, Durán N, et al. Biosynthesis of CdS quantum dots mediated by volatile sulfur compounds released by antarctic *Pseudomonas fragi*. *Front Microbiol* **2019**; 10: 1866. doi: 10.3389/fmicb.2019.01866.
28. Shen L, Wang H, Liu S, Bai Z, Zhang S, Zhang X, et al. Assembling of sulfur quantum dots in fission of sublimed sulfur. *J Am Chem Soc* **2018**; 140: 7878-84. doi: 10.1021/jacs.8b02792.
29. Mousavi SH, Jalili-Nik M, Soukhtanloo M, Soltani A, Abbasinezhad-Moud F, Mollazadeh H, et al. Auraptene inhibits migration, invasion and metastatic behavior of human malignant glioblastoma cells: an in vitro and in silico study. *Avicenna J Phytomed* **2024**; 14: 349-64. doi: 10.22038/ajp.2023.23586.
30. Tajvar Nasab N, Jalili-Nik M, Afshari AR, Rezaei Farimani A, Soukhtanloo M. Urolithin B inhibits proliferation and migration and promotes apoptosis and necrosis by inducing G2/M arrest and targeting MMP-2/-9 expression in osteosarcoma cells. *J Biochem Mol Toxicol* **2023**; 37: e23486. doi: 10.1002/jbt.23486.
31. Wang L, Wang C, Li X, Tao Z, Zhu W, Su Y, et al. Melatonin and erastin emerge synergistic anti-tumor effects on oral squamous cell carcinoma by inducing apoptosis, ferroptosis, and inhibiting

autophagy through promoting ROS. *Cell Mol Biol Lett* **2023**; 28: 36. doi: 10.1186/s11658-023-00449-6.
32. Mirzaei SM, Kazemi Oskuee R, Sadri K, Sabouri Z, Farasati Far B, Abdulabbas HS, et al. Development of a novel sulfur quantum dots: synthesis, 99mTc radiolabeling, and biodistribution. *Appl Biochem Biotechnol* **2024**; 196: 3356-73. doi: 10.1007/s12010-023-04703-7.
33. Shang L, Nienhaus K, Jiang X, Yang L, Landfester K, Mailänder V, et al. Nanoparticle interactions with live cells: quantitative fluorescence microscopy of nanoparticle size effects. *Beilstein J Nanotechnol* **2014**; 5: 2388-97. doi: 10.3762/bjnano.5.248.
34. Li L, Yang C, Li Y, Nie Y, Tian X. Sulfur quantum dot-based portable paper sensors for fluorometric and colorimetric dual-channel detection of cobalt. *J Mater Sci* **2021**; 56: 4782-96. doi: 10.1007/s10853-020-05544-z.
35. Segneanu AE, Gozescu I, Dabici A, Sfirloaga P, Szabadai Z. *Organic Compounds FT-IR Spectroscopy*. Romania: IntechOpen; **2012**.
36. Sebastiammal S, Sonia S, Henry J, Lesly Fathima A. Green synthesis of cerium oxide nanoparticles *using Aloe vera* leaf extract and its optical properties. *Songklanakarin J Sci Technol* **2021**; 43: 582-7. doi: 10.14456/sjst-psu.2021.78.
37. Muthuvel A, Jothibas M, Mohana V, Manoharan C. Green synthesis of cerium oxide nanoparticles using *Calotropis procera* flower extract and their photocatalytic degradation and antibacterial activity. *Inorg Chem Commun* **2020**; 119: 108086. doi: 10.1016/j.inoche.2020.108086.
38. Qiao G, Liu L, Hao X, Zheng J, Liu W, Gao J, et al. Signal transduction from small particles: Sulfur nanodots featuring mercury sensing, cell entry mechanism and in vitro tracking performance. *Chem Eng J* **2020**; 382: 122907. doi: 10.1016/j.cej.2019.122907.
39. Wang C, Wei Z, Pan C, Pan Z, Wang X, Liu J, et al. Dual functional hydrogen peroxide boosted one step solvothermal synthesis of highly uniform sulfur quantum dots at elevated temperature and their fluorescent sensing. *Sens Actuators B Chem* **2021**; 344: 130326. doi: 10.1016/j.snb.2021.130326.
40. Calvache-Muñoz J, Prado FA, Tirado L, Daza-Gomez LC, Cuervo-Ochoa G, Calambas HL, et al. Structural and optical properties of CeO2 nanoparticles synthesized by modified polymer complex method. *J Inorg Organomet Polym Mater* **2019**; 29: 813-26. doi: 10.1007/s10904-018-01056-1.
41. Channei D, Inceesungvorn B, Wetchakun N, Ukritnukun S, Nattestad A, Chen J, et al. Photocatalytic degradation of methyl orange by CeO2 and Fe-doped CeO2 films under visible light irradiation. *Sci Rep* **2014**; 4: 5757. doi: 10.1038/srep05757.
42. Duan Y, Tan J, Huang Z, Deng Q, Liu S, Wang G, et al. Facile synthesis of carboxymethyl cellulose sulfur quantum dots for live cell imaging and sensitive detection of Cr(VI) and ascorbic acid. *Carbohydr Polym* **2020**; 249: 116882. doi: 10.1016/j.carbpol.2020.116882.
43. Muluh TA. Clinical facts on retinoblastoma. *Clin Cancer Drugs* **2024**; 10: E2212697X305434. doi: 10.2174/012212697x305434240807182426.
44. Hatem S, Mohammed D, Ezzat N. Nanotechnology-based strategies overcoming the challenges of retinoblastoma: a comprehensive overview and future perspectives. *Futur J Pharm Sci* **2024**; 10: 14. doi: 10.1186/s43094-024-00587-4.
45. Onugwu AL, Ugorji OL, Ufondu CA, Ihim SA, Echezona AC, Nwagwu CS, et al. Nanoparticle-based delivery systems as emerging therapy in retinoblastoma: recent advances, challenges and prospects. *Nanoscale Adv* **2023**; 5: 4628-48. doi: 10.1039/d3na00462g.
46. Ma F, Zhou Q, Yang M, Zhang J, Chen X. Microwave-assisted synthesis of sulfur quantum dots for detection of alkaline phosphatase activity. *Nanomaterials (Basel)* **2022**; 12: 2787. doi: 10.3390/nano12162787.
47. Sheng Y, Huang Z, Zhong Q, Deng H, Lai M, Yang Y, et al. Size-focusing results in highly photoluminescent sulfur quantum dots with a stable emission wavelength. *Nanoscale* **2021**; 13: 2519-26. doi: 10.1039/d0nr07251f.
48. Tumkur PP, Gunasekaran NK, Lamani BR, Nazario Bayon N, Prabhakaran K, Hall JC, et al. Cerium oxide nanoparticles: synthesis and characterization for biosafe applications. *Nanomanufacturing* **2021**; 1: 176-89. doi: 10.3390/nanomanufacturing1030013.
49. Liu S, Wang H, Feng A, Chang J, Zhang C, Shi YE, et al. Photoluminescence investigations of sulfur quantum dots synthesized by a bubbling-assisted strategy. *Nanoscale Adv* **2021**; 3: 4271-5. doi: 10.1039/d1na00282a.
50. Bortamuly R, Konwar G, Boruah PK, Das MR, Mahanta D, Saikia P. CeO2-PANI-HCl and CeO2-PANI-PTSA composites: synthesis, characterization, and utilization as supercapacitor electrode materials. *Ionics (Kiel)* **2020**; 26: 5747-56. doi: 10.1007/s11581-020-03690-7.
51. Gupta A, Das S, Neal CJ, Seal S. Controlling the surface chemistry of cerium oxide nanoparticles for biological applications. *J Mater Chem B* **2016**; 4: 3195-202. doi: 10.1039/c6tb00396f.
52. Nazaripour E, Mousazadeh F, Doosti Moghadam M, Najafi K, Borhani F, Sarani M, et al. Biosynthesis of lead oxide and cerium oxide nanoparticles and their cytotoxic activities against colon cancer cell line. *Inorg Chem Commun* **2021**; 131: 108800. doi: 10.1016/j.inoche.2021.108800.
53. Datta A, Mishra S, Manna K, Saha KD, Mukherjee S, Roy S. Pro-oxidant therapeutic activities of cerium oxide nanoparticles in colorectal carcinoma cells. *ACS Omega* **2020**; 5: 9714-23. doi: 10.1021/acsomega.9b04006.
54. Feng N, Liu Y, Dai X, Wang Y, Guo Q, Li Q. Advanced applications of cerium oxide based nanozymes in cancer. *RSC Adv* **2022**; 12: 1486-93. doi: 10.1039/d1ra05407d.
55. Alizadeh N, Salimi A, Sham TK, Bazylewski P, Fanchini G. Intrinsic enzyme-like activities of cerium oxide nanocomposite and its application for extracellular H2O2 detection using an electrochemical microfluidic device. *ACS Omega* **2020**; 5: 11883-94. doi: 10.1021/acsomega.9b03252.
56. Hijaz M, Das S, Mert I, Gupta A, Al-Wahab Z, Tebbe C, et al. Folic acid tagged nanoceria as a novel therapeutic agent in ovarian cancer. *BMC Cancer* **2016**; 16: 220. doi: 10.1186/s12885-016-2206-4.
57. Celardo I, De Nicola M, Mandoli C, Pedersen JZ, Traversa E, Ghibelli L. Ce^{3+} ions determine redox-dependent anti-apoptotic effect of cerium oxide nanoparticles. *ACS Nano* **2011**; 5: 4537-49. doi: 10.1021/nn200126a.
58. Ning K, Sun Y, Liu J, Fu Y, Ye K, Liang J, et al. Research update of emergent sulfur quantum dots in synthesis and sensing/bioimaging applications. *Molecules* **2022**; 27: 2822. doi: 10.3390/molecules27092822.
59. Song Y, Tan J, Wang G, Gao P, Lei J, Zhou L. Oxygen accelerated scalable synthesis of highly fluorescent sulfur quantum dots. *Chem Sci* **2019**; 11: 772-7. doi: 10.1039/c9sc05019a.